2021 43rd Annual International Conference of the
IEEE Engineering in Medicine & Biology Society (EMBC)
Oct 31 - Nov 4, 2021. Virtual Conference

Lung contour detection in Chest X-ray images using Mask Region-based Convolutional Neural Network and Adaptive Closed Polyline Searching Method

Tao Peng, Yidong Gu and Jing Wang*

Abstract— **Detection of lung contour on chest X-ray images (CXRs) is a necessary step for computer-aid medical imaging analysis. Because of the low-intensity contrast around lung boundary and large inter-subject variance, it is challenging to detect lung from structural CXR images accurately. To tackle this problem, we design an automatic and hybrid detection network containing two stages for lung contour detection on CXRs. In the first stage, an image preprocessing stage based on a deep learning model is used to automatically extract coarse lung contours. In the second stage, a refinement step is used to fine-tune the coarse segmentation results based on an improved principal curve-based method coupled with an improved machine learning method. The model is evaluated on several public datasets, and experiments demonstrate that the performance of the proposed method outperforms state-of-the-art methods.**

Clinical Relevance— **This can help radiologists for automatic separate lung, which can decrease the workloads of the radiologists' manually delineated lung contour in CXRs.**

I. Introduction

Lung Chest X-ray images (CXRs) are widely used in clinics due to their low cost and low radiation dose. During the COVID-19 outbreak, CXR is considered as a frontline imaging test. Accurate lung Region of Interest (ROI) detection in CXRs is often needed in Computer-Aided Diagnosis (CADx) because it is an important step for diagnosing lung diseases. However, it remains a challenging task for accurate lung segmentation in CXRs due to various reasons, including (1) the overlap between the lung and other anatomical structures (i.e., heart, clavicle bones, and rib cage); (2) edges at the rib cage and clavicle make many minimization methods to get stuck at local minima during optimization, and (3) inconsistencies in anatomical shape between different individuals make segmenting small costophrenic angles challenging.

Many different segmentation methods have been proposed for medical segmentation in CXRs, including (1) threshold segmentation methods, (2) region segmentation methods, and (3) contour detection methods. Ahmad *et al*. [1] proposed a Content Based Medical Image Retrieval System (CBMIRS) for lung segmentation, but the Jaccard Similarity Coefficient (Ω) was only 0.87 when they tested the method on a public dataset. Thomas *et al*. [2] mainly combined the improved GrowCut method for lung tumor segmentation in positron emission tomography. Chen *et al*. [3] presented a lung contour detection method using deep convolutional encoder-decoder architecture (SegNet) and tested on different public datasets, but the Dice Similarity Coefficient (DSC) on the enhanced chest X-ray (ECXR) dataset is only 0.851. Compared with the other methods, the contour detection method easily obtains the shape of the anatomical structure with less time complexity.

The contour detection method is mainly used to approximate the contour of tissues by using region expression or curve description. In Ref. [4], Farhangi *et al*. designed a lung nodule segmentation method using Sparse Linear Combination of Training Shapes (SCoTS). However, the performance of this proposed model strongly depends on the diversity and accuracy of the training shapes. Li *et al*. [5] proposed a lung nodule detection in CXRs using the multi-resolution convolutional networks, while Peng *et al*. [6] proposed a hybrid method combining the principal curve-based method and machine learning-based network for lung segmentation.

In this study, we propose a hybrid lung contour detection method in CXRs. Our main contributions are summarized as follows: (1) a hybrid network is proposed for lung contour detection that automatically achieves not only the overall lung contours but also the ROI contours. (2) Compared with our previous works [7], we propose an improved Adaptive Closed Polyline Searching Method (ACPSM) to filter the abnormal vertices using different normalization methods and adding a new vertices cleaning method; (3) Compared with Leema *et al*. [8], we use a new memory-based mechanism to store the best parameters from the previous cycle and then use them as the initial value for the next cycle. Moreover, in the mutation step, we use multi-mutation operators for generating the new mutant individual. (4) To express the lung ROI contour, to the best of our knowledge, a smooth mathematical model is used for the first time, which is represented by the parameters of the machine learning method.

This research was supported by the Cancer Prevention and Research Institute of Texas (RP160661).

Tao Peng and Jing Wang* are with the Department of Radiation Oncology, Medical Artificial Intelligence and Automation Laboratory, University of Texas Southwestern Medical Center, 2280 Inwood Road, Dallas, TX, USA. (e-mail: sdpengtao401@gmail.com; Jing.Wang@utsouthwestern.edu).

Yidong Gu is with Department of Medical Ultrasound, The Affiliated Suzhou Hospital of Nanjing Medical University, Suzhou Municipal Hospital, Suzhou 215002, Jiangsu, China (e-mail: guyidong850820@aliyun.com).

Tao Peng and Yidong Gu contribute equally to this work.

* Corresponding author: Jing Wang

II. METHOD

A. Detection Framework

For accurate lung contour detection, we develop a coarse-to-fine cascade network, where coarse segmentation is achieved by using Mask-RCNN [9] with data augmentation (Stage 1), and the optimization step that combines an improved ACPSM with an improved Adaptive Memory-based Differential Evolution-Backpropagation Neural Network Method (AMDE-BNNM) (Stage 2). The flowchart of the proposed method is shown in Figure 1. Furthermore, we add input/output of each step of the proposed method in TABLE I.

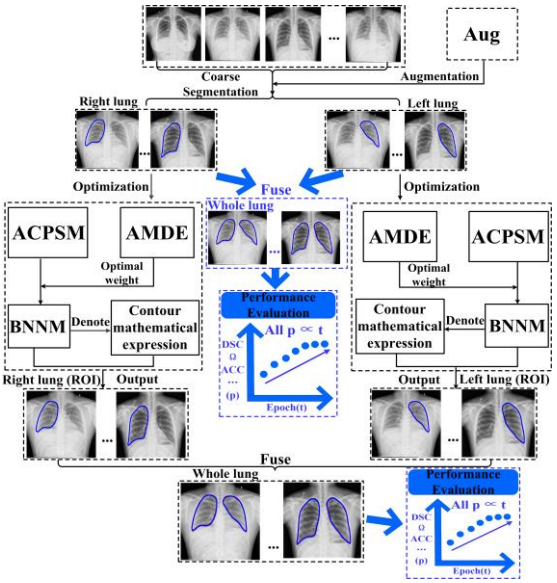

Figure 1. The flowchart of the proposed method. After augmentation, we annotate the ROIs (i.e., left and right lung), respectively. Then, the Mask-RCNN is used for the coarse segmentation for each ROI, and the optimization method is used for fine-tuning the coarse segmentation results of each ROI. Finally, we fuse the segmentation results of both left and right ROIs of the same slice, where we extract the coordinates of both ROIs' segmentation results and overlay to the raw slice, and achieve the whole lung's results. After segmentation, we evaluate the final results quantitatively and qualitatively.

TABLE I

INPUT/OUTPUT OF EACH STEP OF PROPOSED METHOD

Method	Input	Output
Mask R-CNN	Raw data	Coarse segmentation result
ACPSM	Coarse segmentation result (points)	Data sequences (points and corresponding projection indexes)
AMDE	Initial parameters (shown in Stage 2)	Optimal initial weight of BNNM
BNNM	Data sequences	Refined result

Stage 1: Coarse segmentation

Considering that the Mask R-CNN is a good choice for automatically segmenting objects, we use it as the coarse segmentation step. The main network architecture of the Mask-RCNN can be found in Ref. [9]. In this work, we use the rotation method for data augmentation, where each original image was rotated by 45°, 90°, 135°, 180°, 225°, 270°, and 315° until they reached the expected number of the augmented images.

Stage 2: Optimization

The optimization step is mainly used to refine the coarse segmentation results, which combines the improved ACPSM and Improved AMDE-BNNM.

Improved ACPSM We have previously developed a semi-automatic method [7] termed Closed Polyline Searching Method (CPSM) that added several constraint conditions based on Polygonal Line Method (PLM) [6] for medical imaging segmentation. In this work, we proposed the ACPSM, shown in Figure 2.

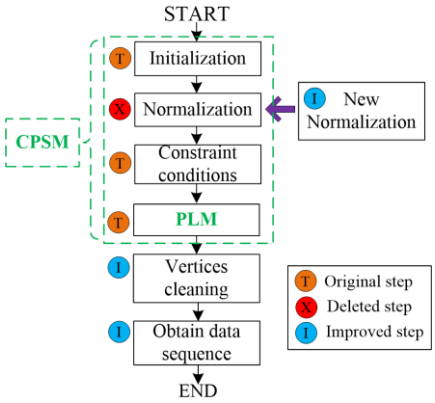

Figure 2. The flowchart of the proposed ACPSM. Furthermore, the definition of data sequence can be found in Ref. [6].

Compared with our previous work, the ACPSM presented in this work mainly has two improvements: (1) we use a new normalization step with stronger anti-interference to replace the Min-Max normalization method; and (2) furthermore, we add a new vertices cleaning method for filtering the abnormal vertices and detailed steps are summarized as following: we set the vertices cleaning Flag(v_i) is 1 when (ls_{i-1} or ls_i)>r, where ls_i is the length of the i-th line segment, and r is the data radius; Otherwise, Flag(v_i)=0. Furthermore, ls_i should meet the following condition,

$$l_{si} = \left\| v_{i+1} - v_i \right\| \quad 1 \le i \le m \tag{1}$$

where m is the number of vertices of the principal curve.

Moreover, two new constraint conditions are newly added to clean the abnormal vertices. If either the following conditions are satisfied, the vertex v_i will be removed: (1) vertex v_i is outside the radius of the data points. (2) Too few sample points are projected to the vertex v_i and neighboring segment consisting of v_i and nearest vertex v_{i+1}, where the number of the data points is close to zero.

Improved AMDE-BNNM Due to the training results of the learning method (i.e., BNNM) strongly depend on the initial parameters (i.e., weight), we use the AMDE to search the optimal initial weight for the BNNM. Then we use BNNM's parameters to express the smooth mathematical model of the lung ROI contour.

Compared with Leema *et al.* [8], we use a memory-based mechanism and an improved mutation step. The main steps of AMDE is as following: ***First***, we initialize the mutation Factor (F), Crossover Rate (CR), present iteration number (G), and max iteration number (GMax). ***Second***, in the improved mutation step, we let x_{rk}^G be the initial candidate, N_p is the

number of solutions, r_k is a random integer in the range of [1, N_p]; and p_G is the probability of using the mutation operator. The mutant individual v_s^{G+1} is generated as below,

$$V_s^{G+1}=\begin{cases} x_{r_1}^G+\text{rand}_1\times(x_{r_2}^G-x_{r_3}^G), & \text{if rand}[0,1]<p_G \\ x_{r_1}^G+\text{rand}_2\times(x_{r_2}^G-x_{r_3}^G)+\text{rand}_3\times(x_{r_4}^G-x_{r_5}^G), & \text{otherwise} \end{cases} \quad (2)$$

Third, we use both the crossover and selection step, according to Ref. [8]. ***Fourth***, the set of all successful crossover probabilities (S_{CR}) and mutation factors (S_F) are selected, respectively, according to the Lehmer function. ***Fifth***, mean mutation Factor (uF) and mean Crossover Rate (uCR) are updated by using S_F and S_{CR}, respectively. ***Sixth***, if present iteration number G⩾GMax, the best candidate is selected as the initial weight of the next BNNM.

After determining the initial weight of the BNNM by the AMDE, we will train the BNNM. In the BNNM, we use a three-layer network. The output layer of the BNNM contains two units, corresponding to x and y, where x and y can be treated as the continuous functions c(x(t)) and c(y(t)), respectively, on projection index t [7]. Two output neurons c(•) of the BNNM can be described as follows,

$$c(t)=\big(c(x(t)),c(y(t))\big)=\Bigg(\frac{e^{\sum_{i=1}^{Z}\frac{1}{1+e^{-(t\omega_i-T_i)}}v_{i,1}-b_1}-e^{-(\sum_{i=1}^{Z}\frac{1}{1+e^{-(t\omega_i-T_i)}}v_{i,1}-b_1)}}{e^{\sum_{i=1}^{Z}\frac{1}{1+e^{-(t\omega_i-T_i)}}v_{i,1}-b_1}+e^{-(\sum_{i=1}^{Z}\frac{1}{1+e^{-(t\omega_i-T_i)}}v_{i,1}-b_1)}},\ \frac{e^{\sum_{i=1}^{Z}\frac{1}{1+e^{-(t\omega_i-T_i)}}v_{i,2}-b_2}-e^{-(\sum_{i=1}^{Z}\frac{1}{1+e^{-(t\omega_i-T_i)}}v_{i,2}-b_2)}}{e^{\sum_{i=1}^{Z}\frac{1}{1+e^{-(t\omega_i-T_i)}}v_{i,2}-b_2}+e^{-(\sum_{i=1}^{Z}\frac{1}{1+e^{-(t\omega_i-T_i)}}v_{i,2}-b_2)}}\Bigg) \quad (3)$$

where t is the projection index, and Z is the number of hidden neurons. w_i(i=1,2,…,Z) and $v_{i,u}$(i=1,2,…,Z; u=1,2) are the weights from input layer to the i-th hidden neuron and from the i-th hidden neuron to the u-th output neuron, respectively. b_u(u=1,2) is the thresholds of the u-th output neuron. T_i(i=1,2,…,Z) is the thresholds of the i-th hidden neuron.

The proposed mathematical expression of lung ROI (i.e. left or right lung) contour can be obtained as follows.

$$f(t)=\big(x(c(x(t))),y(c(y(t)))\big)=\Bigg(\frac{c(x(t))+1-\sqrt{1-(c(x(t)))^2}}{2*c(x(t))},\ \frac{c(y(t))+1-\sqrt{1-(c(y(t)))^2}}{2*c(y(t))}\Bigg) \quad (4)$$

where x(c(x(t))) and y(c(y(t))) denote the x-axis and y-axis coordinate of the contour points, respectively.

B. Materials

In this work, we evaluated the proposed method using three different CXR datasets, ShenZhen hospital Chest X-ray dataset (SZCX) [6], Japanese Society of Radiological Technology dataset (JSRT) [6], and Montgomery County chest X-ray dataset (MC) [6], where SZCX, JSRT, and MC contain 662, 247, 138 CXRs, respectively. All the CXRs were rescaled to 512×512, and the ground truths are marked and verified by three board-certified radiologists. In the optimization step of our proposed method, the mathematical expression of lung ROI is denoted by the BNNM, where we set 10 neurons and 1000 epochs based on our previous work [7] for the BNNM to simplify the complex model and avoid overfitting.

III. RESULTS

We firstly split the SZCX and used 400 of them for training, 162 for validation, and the other 100 for testing. To obtain high accuracy, we use the rotation step to augment training data to 1200 images. Meanwhile, we set 120 epochs and used the COCO pre-trained weight for the Mask-RCNN. Figure 3 shows the quantitative results of different methods on 100 SZCX testing cases. Furthermore, we randomly selected one representative case for evaluation as shown in Figure 4.

ACPSM-BNNM and ACPSM-AMDE-BNNM are principal curve-based and use 400 raw SZCXs for training. Meanwhile, they are semi-automatic models with as little as 30% of the manually delineated points as inputs. The proposed method is the automatic and hybrid method consisting of the principal curve-based and deep learning-based methods.

As shown in Figure 3, we can see that all the methods obtain reasonable lung segmentation, where the DSCs of all the methods are higher than 90%. Compared with ACPSM-BNNM (92.6%), ACPSM-AMDE-BNNM (93.39%) has a higher DSC, and the main reason is that the AMDE is used to select the optimal initial weight for improving the performance of the BNNM. Compared with the deep learning-based method (Mask-RCNN) (94.8%, 1200 training data), the principal curve-based method ACPSM-AMDE-BNNM (93.39%, 400 training data) uses fewer training data and obtains a slightly lower DSC, which demonstrates that the principal curve-based method has a good ability to fit the data accurately. Overall, our proposed method has obtained good performance.

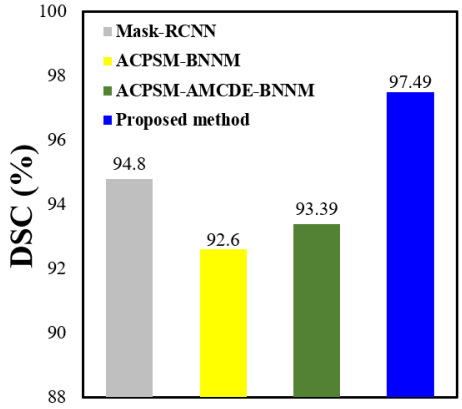

Figure 3. Performance results of different methods on SZCX testing cases

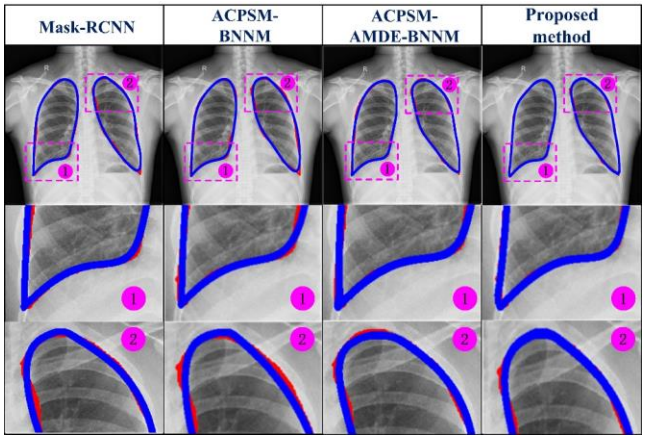

Figure 4. Representative segmentation results for the whole lung. The red lines represent the ground truths, and the blue lines represent the

experimental results. Both the second and third rows show the region of interest of the first-row results.

To prove the generalizability of our method, we use the obtained model trained on SZCX to test the other two public JSRT and MC datasets. TABLE II shows the comparison of the average DSC of the whole lung between our method and several other methods. We used the same training, validation, and testing sets in all the models, where 1200 SZCXs (after augmentation) were used for training, 162 SZCXs for validation, and two different entire datasets (247 JSRTs and 138 MCs) for testing. All the CPSM-BNNM, Hull-CPLM, and DBN-CPL are semi-automatic models with as little as 30% of the manually delineated points as inputs. Others are automatic models and use the raw slices directly. Results summarized in TABLE II show that our proposed method has the best performance among all the models. SD means standard deviation.

TABLE II

QUANTITATIVE COMPARISON WITH THE STATE-OF-THE-ART METHODS.

Reference	Method	Model	Dataset	DSC	*p*-value (Wilcoxon test)
[7]	CPSM-BNNM	Hybrid	JSRT	91.3%± 0.11	0.015
			MC	89.5%± 0.13	0.016
[10]	Hull-CPLM	Hybrid	JSRT	96.5%± 0.02	<0.001
			MC	95.7%± 0.02	<0.001
[6]	DBN-CPL	Hybrid	JSRT	96.6%± 0.02	<0.001
			MC	96.2%± 0.02	<0.001
[11]	Faster-RCNN	Deep learning	JSRT	93.3%± 0.05	0.007
			MC	92.6%± 0.06	0.009
[12]	UNet++	Deep learning	JSRT	95.69%± 0.02	0.004
			MC	95.01%± 0.04	0.007
Proposed method	Proposed method	Hybrid	JSRT	97.2%± 0.01	<0.001
			MC	97%± 0.02	<0.001

IV. CONCLUSION

In this work, a hybrid method is presented for lung segmentation on CXRs. Results show that the better accuracy of our proposed method against state-of-the-art methods. Future work can be focused on the evaluation of different modalities or different organs.

ACKNOWLEDGMENT

The authors acknowledge the funding support from the Cancer Prevention and Research Institute of Texas (RP160661).

REFERENCES

[1] W. Ahmad, W. Zaki, and M. Ahmad Fauzi, "Lung segmentation on standard and mobile chest radiographs using oriented gaussian derivatives filter," *BioMed. Eng. OnLine*, vol. 14, no. 1, pp. 1–26, 2015.

[2] H. M. T Thomas, D. Devakumar, B. Sasidharan, S. R. Bowen, D. K.Heck, and E. James Jebaseelan Samuel, "Hybrid positron emission tomography segmentation of heterogeneous lung tumors using 3d slicer: improved growcut algorithm with threshold initialization," *J. Med. Imaging*, vol. 4, no. 1, p. 011009, 2017.

[3] H. J. Chen, S. J. Ruan, S. W. Huang, and Y. T. Peng, "Lung x-ray segmentation using deep convolutional neural networks on contrast-enhanced binarized images," *Mathematics*, vol. 8, no. 4, p. 545, 2020.

[4] M. M. Farhangi, H. Frigui, A. Seow, and A. A. Amini, "3-d active contour segmentation based on sparse linear combination of training shapes (scots)," *IEEE Trans. Med. Imaging*, vol. 36, no. 11, pp. 2239–2249, 2017.

[5] X. Li, L. Shen, X. Xie, S. Huang, Z. Xie, X. Hong, and J. Yu, "Multi-resolution convolutional networks for chest x-ray radiograph based lung nodule detection," *Artif. Intell. Med.*, vol. 103, p. 101744, 2020.

[6] T. Peng, T. C. Xu, Y. Wang, and F. Li, "Deep Belief Network and Closed Polygonal Line for Lung Segmentation in Chest Radiographs," *Comput. J.*, 2020.

[7] T. Peng, Y. Wang, T. C. Xu, L. Shi, J. Jiang, and S. Zhu, "Detection of lung contour with closed principal curve and machine learning," *J. Digit. Imaging*, vol. 31, no. 4, pp. 520–533, 2018.

[8] N. Leema, H. K. Nehemiah, and A. Kannan, "Neural network classifier optimization using differential evolution with global information and back propagation algorithm for clinical datasets," *Appl. Soft. Comput.*, vol. 49, pp. 834–844, 2016.

[9] K. He, G. Gkioxari, P. Dollar, and R. Girshick, "Mask r-cnn," in *Proceedings of the IEEE international conference on computer vision*, 2017, pp. 2961–2969.

[10] T. Peng, Y. Wang, T. C. Xu, and X. Chen, "Segmentation of lung in chest radiographs using hull and closed polygonal line method," *IEEE Access*, vol. 7, pp. 137794–137810, 2019.

[11] S. Ren, K. He, R. Girshick, and J. Sun, "Faster r-cnn: Towards real-time object detection with region proposal networks," *IEEE Trans. Pattern Anal. Mach. Intell.*, vol. 39, no. 6, pp. 1137–1149, 2017.

[12] Z. Zhou, M. M. Rahman Siddiquee, N. Tajbakhsh, and J. Liang, "Unet++: A nested u-net architecture for medical image segmentation," in *Deep Learning in Medical Image Analysis and Multimodal Learning for Clinical Decision Support*, 2018, pp. 3–11.